CESARE'17
COORDINATING ENGINEERING FOR SUSTAINABILITY AND RESILIENCE
Dead Sea, Amman, Jordan
3-8 May 2017
JORDAN UNIVERSITY OF SCIENCE & TECHNOLOGY
IRBID - JORDAN

# FINITE ELEMENT MODELLING OF TENSILE AND COMPRESSIVE PRESTRESSED TUBULAR MEMBERS

**Michaela Gkantou[1], Marios Theofanous[1] and Charalampos Baniotopoulos[1]**
[1]School of Engineering (Department of Civil Engineering, University of Birmingham, Edgbaston B15 2TT, UK)
e-mail: m.gkantou@bham.ac.uk

**Keywords:** FE, Prestress, Tubular, Grout, High Strength Steel (HSS)

**Abstract.** *The current paper discusses the simulation of the structural behaviour of prestressed tubular members in steel grade S460 and S690, through the execution of advanced numerical modelling. Numerical models are validated against published experimental data [1], in which different initial prestress levels and the presence of grouting has been examined for high strength steel compressive and tensile members. In order to accurately replicate the experimental response through finite element modelling, certain parameters oblige careful consideration. The selected numerical solver, the material models and the element types are therefore thoroughly described in the present paper. Upon establishment of the numerical models, the numerically generated ultimate loads, failure modes and the full load-deformation curves are compared with the experimental ones, indicating a successful validation. For the compressive members, an imperfection study is executed in order to investigate the influence of the initial geometric imperfections on the overall structural performance, showing that an imperfection magnitude of L/1000 predicts sufficiently the experimental behavior. Evaluating both the experimental and the numerical results, it is concluded that, as anticipated, prestressing enhances the load-bearing capacity for tensile members, whilst is detrimental for compressive members.*

## 1 INTRODUCTION

In order to allow for long spans with reduced cross-sectional dimensions, prestressing has been extensively applied in concrete structures. Besides prestressed concrete, prestressing has been shown beneficial to steel structures. A series of long span steel structures that exploit the advances offered by the use of prestress have already been developed [2]. To better comprehend the structural response of prestressed steel structures, research interest has been attracted [1, 3-5]. Focus hereafter is based on tubular prestressed steel structures, in which cables are housed within the hollow sections, offering a practical means of prestressing.

Aiming to allow for enhanced material savings, the gains in strength and stiffness due to the application of prestress [5] could be combined with the benefits arising from the use of higher steel grades [6]. Towards this direction, the present study investigates the structural performance of prestressed members employing square hollow sections in high strength steel grades. In particular, focus is placed upon S460 and S690 prestressed members subjected to axial loading. The considered members could comprise bottom chord truss elements which are subjected either to tension or to compression depending on the assigned loading, i.e. vertical loading or uplift respectively. The structural performance of the prestressed members is investigated by means of numerical modelling.

## 2 DEVELOPMENT OF THE FINITE ELEMENT MODELS

The current section provides a detailed description of the finite element (FE) models which have been generated with the general purpose FE package Abaqus [7]. The experimental programme [1] upon which the validation of the FE models was based is briefly discussed in Subsection 2.1. Subsections 2.2-2.5 provide numerical modelling

assumptions including the employed material models, element types, constraints, boundary conditions and interaction properties. The numerical application of the initial prestress load, the introduction of the initial geometric imperfections and the type of analysis performed are explained in Subsections 2.6, 2.7 and 2.8 respectively.

### 2.1 Brief description of the experimental programme

The experimental programme utilized for the validation of the FE models studied herein was conducted at the structures lab of Imperial College London and comprised a series of prestressed tubular members tested to failure under tensile or compressive loading [1]. The specimens employed 50×50×5 hollow sections in S460 and S690 steel grades. The tensile members were two meters long, whilst the compressive members were one meter long. For the prestressed members, a 7-wire strand, with cross-sectional area 150 $mm^2$ and nominal tensile strength 1860 $N/mm^2$, was housed inside the hollow section. In order to ensure that the tubular members would not buckle under initial prestress, connecting collars were also attached to the cables.

For the tensile members (T), the following four prestress levels were studied for both considered steel grades: (i) no cable (NG), (ii) a cable with $P_{nom}$ prestress (NG0), (iii) a cable with $0.5P_{opt}$ prestress (NG1) and (iv) a cable with $P_{opt}$ prestress (NG2). Note that $P_{nom}$ prestress corresponds to a nominal prestress load to remove slack from the cable, whilst $P_{opt}$ is the optimal prestress level for which both the tube and the cable yield simultaneously under tensile loading and is given from Eq. (1) [3]

$$P_{opt} = \left(\frac{A_c A_t}{A_t E_t + A_c E_c}\right)\left(f_{cy} E_t - f_{ty} E_c\right) \quad but\ P_{opt} \le A_t f_{yt} \ \ and \ \ A_c f_{yc} \tag{1}$$

where $A$, $E$ and $f_y$ are the cross-sectional area, Young's modulus and yield strength; the subscripts $c$ and $t$ refer to the cable and surrounding steel tube respectively. Strands' breakage combined with tube's necking was the observed failure mode for the prestressed tensile members.

For the compressive steel members (C), the following two levels were investigated: (i) no cable (NG) and (ii) a cable with $P_{opt}$ prestress (NG2). The compressive members primarily failed by global buckling.

In order to ensure good bonding properties and corrosion resistance, grouting can be added within the tube of the members. For prestressed members subjected to tensile loading, the addition of concrete is awaited to slightly improve the system's overall performance, whilst the combination of concrete's increased compressive resistance with steel's considerable tensile strength is expected to allow for improved performance in the compressive members. To evaluate grouting's effect to the structural response, two prestress levels, namely $0.5P_{opt}$ (G1) and $P_{opt}$ (G2), were considered for the tensile grouted members (T) and three prestress levels, namely $P_{nom}$ (G0), $0.5P_{opt}$ (G1) and $P_{opt}$ (G2), for the compressive grouted members (C). Note that NG and G stands for non-grouted and grouted members respectively.

### 2.2 Material models

Material modelling was based on a series of coupon tests. For the steel tubes, the average material response as extracted from S460 and S690 tensile coupon tests [6] and shown in Figure 1(a) has been adopted. For the cables, material tests found an average yield stress and Young's modulus equal to 1700 $N/mm^2$ and 130000 $N/mm^2$ respectively. Note that tests on cables of different lengths resulted in an apparent variation in the cable's effective modulus. Upon application of a 2-stage Ramberg-Osgood model according to the equations provided in [8], the extracted stress-strain curves are shown in Figure 1(b). For the steel collars, an elastic-perfectly plastic response, as shown in Figure 1(c) has been assumed. For the steel tubes, the cable and the collars, the von Mises yield criterion with isotropic hardening, that has been seen to accurately represent the behavior of metallic materials, has been applied.

The numerical simulation of concrete is known to be more challenging. In order to model concrete's failure both in compression and in tension, including recognition of the crack pattern, Abaqus provides different material models. For the present study, it was found adequate to simulate the grouting with concrete damaged plasticity (CDP) constitutive model [7]. CDP assumes that the tensile cracking and the compressive crushing are the failure mechanisms, whereas the uniaxial tensile and compressive behaviour is characterized by damaged plasticity. The values introduced for the angle of dilation $\theta$, the eccentricity, the ratio of equibiaxial to uniaxial compressive stress

$f_{b0}/f_{c0}$, the ratio of the second stress invariant on the tensile meridian to that on the compressive meridian at initial yield and the viscosity parameter were 40, 0.1, 1.16, 0.666 and 0 respectively, in line with [9]. The Young's modulus $E$ and tensile strength $f_{ct}$ were determined according to ACI [10], whilst Poisson's ratio was assumed equal to 0.2. The compressive stress-strain response was formulated according to the recommendations provided in [9] as shown in Figure 1(d), considering compressive strength equal to 48 $N/mm^2$. The tension stiffening behaviour was defined in terms of tensile stress and axial deformation, considering fracture energy equal to 0.09. The influence of the assumed values for the dilation angle and the fracture energy was preliminary studied, revealing minor variation in the attained response for different employed values for the aforementioned quantities.

Note that damage properties have not been included in any of the material models. The stress-strain curves were converted into the true stress-logarithmic plastic strain format before their input into the software.

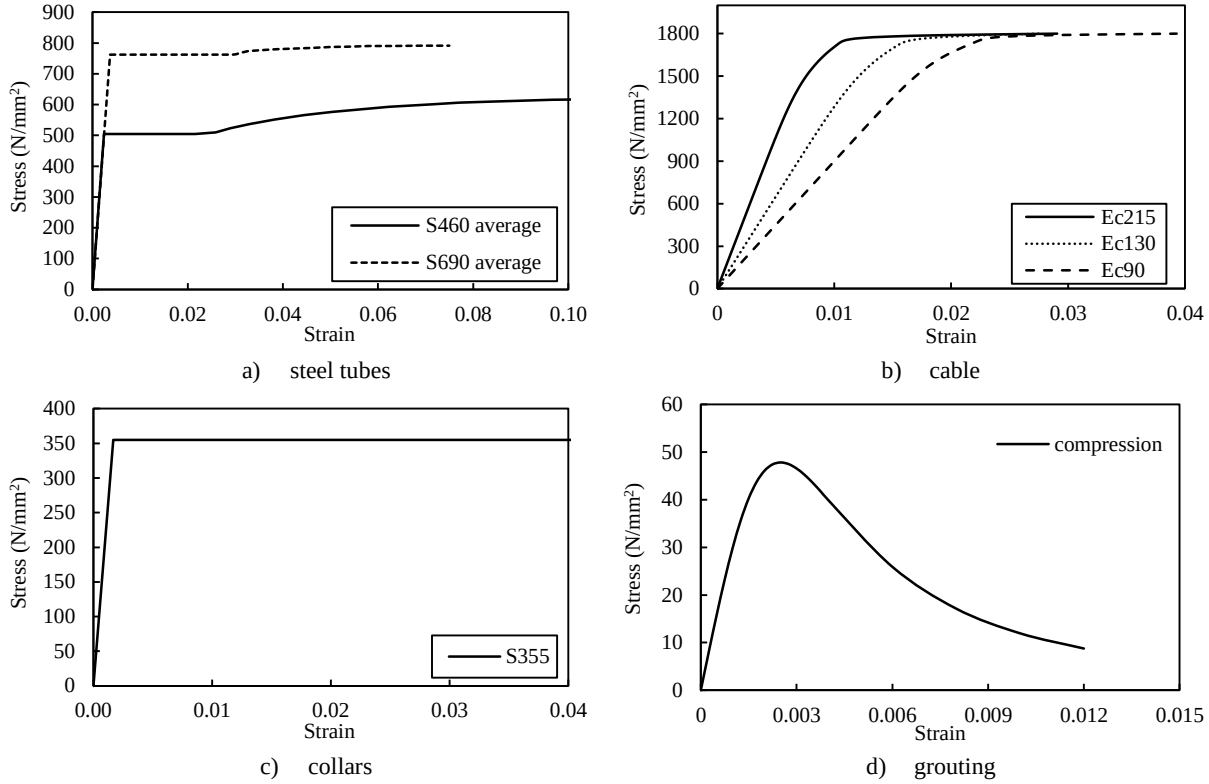


a) steel tubes b) cable

c) collars d) grouting

Figure 1. Material properties.

### 2.3 Element types

In FE modelling, the structural parts can be simulated with different element types. An initial study examined the behaviour of non-grouted prestressed members for the following three cases of employed FE element types:

(i) shell elements for the tube, beam elements for the cable, tie constraint for the collars' representation
(ii) shell elements for the tube, solid elements for the cable, solid elements for the collars
(iii) shell elements for the tube, solid elements for the cable, solid elements for the collars

Similar response was achieved for all the studied cases. Given that the concrete of grouted members will be simulated with solid elements and in order to maintain consistency between grouted and non-grouted models, it was decided to further investigate model (iii). Three solid elements were applied along the thickness of the steel tubes. For the simulation of the cable, the 7-strand wire was simplified to a circular solid beam with cross-sectional area equal to 150 $mm^2$. An initial mesh convergence study was performed to ensure accuracy whilst keeping computational time to minimum.

### 2.4 Constraints & boundary conditions

In both the compressive and tensile members, a rigid body was assigned in the section's ends and the motion was constrained to a reference point (RP). In tensile members, all degrees of freedom were restrained at the RPs, except for the translational degree of freedom along the longitudinal axis that was left free in one of the two ends. In compressive members, the rotational degrees of freedom around the two transverse member's axes were also left free at the RPs of the section's ends. In order to reduce the required computational time, symmetry in geometry was exploited. Half of the structural system was modelled along the longitudinal axis and appropriate symmetry boundary conditions were assigned. A typical developed FE model is shown in Figure 2.

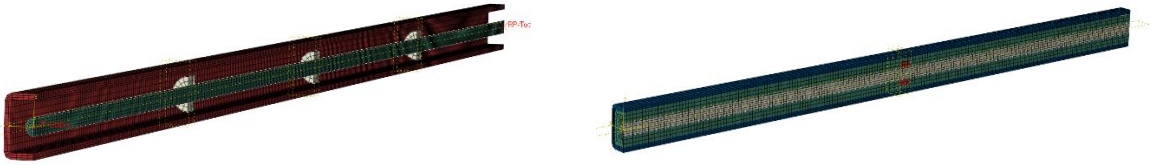

a) Tensile non-grouted member b) Compressive grouted member

Figure 2. Typical finite element models.

### 2.5 Interaction properties

The collars were welded to the cable and hence the tie constraint was sufficient for simulating their interaction. For the contact emerging between (i) tube-cable and (ii) tube-collar in non-grouted members and between (i) grouting-collar (ii) grouting-tube and (iii) grouting-cable in grouted members, the general contact algorithm of Abaqus [7] was applied. For normal contact, the "hard" contact relationship that minimizes the penetration has been adopted. A friction coefficient was employed to define the tangential behaviour over contacting surfaces. A preliminary parametric study found small effect of the frictional coefficient on the overall performance. In line with [9], a friction coefficient equal to 0.3 was adopted for the tangential contact behaviour.

### 2.6 Initial prestress

The stresses arising due to prestress were introduced through an initial static analysis. The extracted stress state was inserted as a predefined field in the subsequent nonlinear analysis. The method of introducing the prestress as a predefined temperature field has also been found in literature [3] but the simpler, nevertheless efficient, method of executing an initial static analysis was preferred.

### 2.7 Geometric imperfections & residual stresses

In order to incorporate the initial geometric imperfections in the structural system, a linear buckling analysis was initially performed and the extracted buckling mode corresponding to the observed failure mode was introduced in the subsequent nonlinear analysis. Residual stresses were of low magnitude for the considered hollow sections [6] and thus were not explicitly modelled.

### 2.8 Analysis techniques

Implicit solvers, in which a number of iterations are executed in order to evaluate the load-displacement equilibrium by solving a set of equations, are commonly applied to simulate nonlinear static problems. Even though this method appeared suitable for the compressive non-grouted specimens, the combined material, geometric and contact nonlinearities made convergence difficult for the tensile grouted members. For this reason and in order to keep consistency within the whole study, the explicit solver, in which the response is obtained incrementally by explicitly advancing the kinematic state from the previous increment, was applied for the analyses hereafter. To ensure static loading, it was guaranteed that the kinetic energy (ALLKE from Abaqus) was only a very small fraction (less than 5%) of the total energy (ALLIE from Abaqus). The analyses were executed at the BlueBear

Cluster possessed by the University of Birmingham. In order to reduce the computational time, mass scaling values, ensuring stable time increments in function of the employed elements' size, were also adopted. In order to avoid oscillations after buckling occurrence, large values of time periods needed to be applied in the compressive members. It is worth mentioning that prestressed compressive elements exhibited oscillated response during the first iterations owing to the resistance to buckling provided by the tensioned cables.

## 3 VALIDATION OF THE FINITE ELEMENT MODELS

Adopting the modelling assumptions described in Section 2, the current section presents the validation of the generated finite element models. In particular, Subsection 3.1 provides the comparison of the experimental and numerical response of the tensile members. Subsection 3.2 focuses on the compressive members and executes an imperfection study to find the magnitude that achieves closest match with the test data. The obtained results are discussed in Subsection 3.3.

### 3.1 Tensile prestressed members

Upon execution of nonlinear static analysis for the tensile members, the numerically obtained ultimate loads $N_{u,FE}$ were extracted and compared with the experimental ones $N_{u,Exp}$. The results are shown in Table 1, where an excellent validation can be seen. The load-deformation response of typical cases is also shown in Figure 3. A very well replication of the overall response can be observed. Emphasis is worth to be placed on the following three points.

(i) For the cable of prestressed members, the effect of all three assumed material models of Figure 1(b) was investigated. The employed cable's effective properties were found to have considerable influence on the $P_{nom}$ prestressed members and smaller influence on members with larger prestress loads. Best replication of the load-axial displacement curve was found for young's modulus equal to 130000 $N/mm^2$. The curves shown in Figure 3 correspond to this value.

(ii) The load-deformation curves of the grouted members depicted in Figures 3(b) and 3(d) were found to be more ductile compared to their counterparts without any grouting, showing that the existence of concrete delays global buckling, allowing the failure to occur in larger strains.

(iii) The continuous drops in the experimental curve of Figure 3(c) reflect successive cables' breakage. This could have been captured numerically with explicit modelling of the strands according to [11], ensuring adequate mesh refining, appropriate contact modelling, attention to damage material properties and advanced computational resources, but was out of scope of the present study.

Table 1. Tensile specimens - Comparison of numerical and experimental ultimate loads.

| Specimen | $N_{u,FE}/N_{u,Exp}$ |
|---|---|
| T460NG | 1.02 |
| T460NG0 | 1.06 |
| T460NG1 | 0.98 |
| T460NG2 | 1.04 |
| T460G1 | 0.98 |
| T460G2 | 0.95 |
| T690NG | 0.94 |
| T690NG0 | 0.98 |
| T690NG1 | 0.94 |
| T690NG2 | 0.97 |
| T690G1 | 0.93 |
| T690G2 | 0.94 |
| Mean | 0.98 |
| COV | 0.04 |

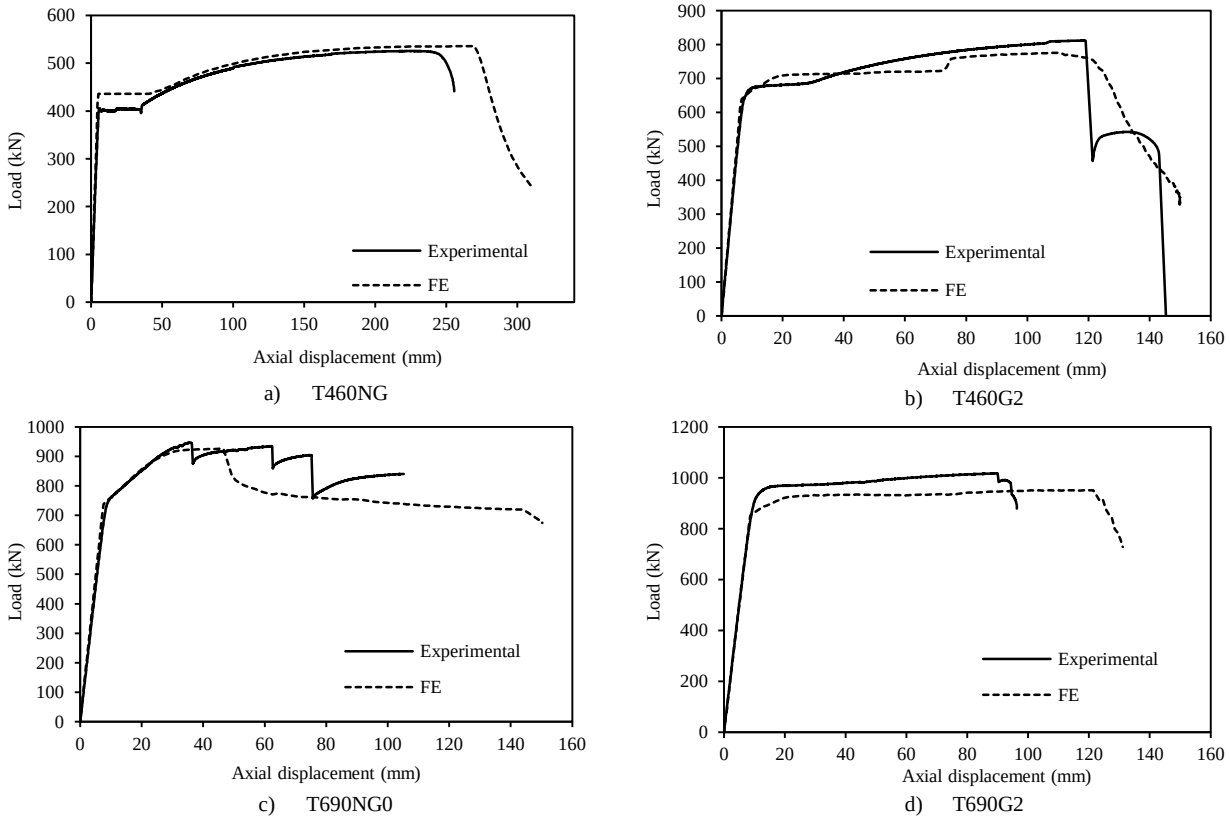


Figure 3. Tensile specimens - Comparison of numerical and experimental load-deformation response.

### 3.2 Compressive prestressed members

The compressive specimens are expected to fail by global buckling and hence the amplitude of the initial geometric imperfections affects the ultimate response. In order to find the imperfection magnitude that results in the best agreement with the experimental results, the following six magnitudes were investigated: (i) measured imperfection magnitudes, as given in [1], (ii) $L/3000$, (iii) $L/2000$, (iv) $L/1500$, (v) $L/1000$ and (vi) $L/750$, where $L$ the member's length. The numerically generated ultimate loads were compared with the experimental ones, as shown in Table 2. As can be seen, best agreement with a mean value of $N_{u,FE}/N_{u,Exp}$ 0.97 and quite high but still acceptable coefficient of variation, was achieved for the magnitude $L/1000$. The load-deformation response for the considered imperfection magnitudes was also recorded, demonstrating overall good agreement with the test response, as shown for typical cases in Figure 4.

Table 2. Compressive specimens - Comparison of numerical and experimental ultimate loads for six geometric imperfection magnitudes.

| Specimen | $N_{u,FE}/N_{u,Exp}$ | | | | | |
|---|---|---|---|---|---|---|
| | Imperfection Magnitude | | | | | |
| | Exp | L/3000 | L/2000 | L/1500 | L/1000 | L/750 |
| G460NG0 | 1.02 | 1.08 | 1.06 | 1.05 | 1.00 | 0.96 |
| G460NG2 | 0.90 | 1.12 | 1.01 | 1.01 | 0.95 | 0.91 |
| G460G0 | 1.10 | 1.16 | 1.14 | 1.11 | 1.04 | 1.00 |
| G460G1 | 1.17 | 1.33 | 1.28 | 1.25 | 1.19 | 1.15 |
| G460G2 | 1.17 | 1.30 | 1.17 | 1.17 | 1.14 | 1.06 |
| G690NG0 | 0.95 | 0.96 | 0.95 | 0.94 | 0.92 | 0.91 |
| G690NG2 | 0.88 | 0.91 | 0.89 | 0.88 | 0.86 | 0.83 |
| G690G0 | 0.91 | 0.91 | 0.90 | 0.88 | 0.86 | 0.84 |
| G690G1 | 0.93 | 1.02 | 1.00 | 0.99 | 0.96 | 0.94 |
| G690G2 | 0.88 | 0.83 | 0.80 | 0.80 | 0.78 | 0.76 |
| Mean | 0.99 | 1.06 | 1.02 | 1.01 | 0.97 | 0.93 |
| COV | 0.12 | 0.16 | 0.14 | 0.14 | 0.13 | 0.12 |

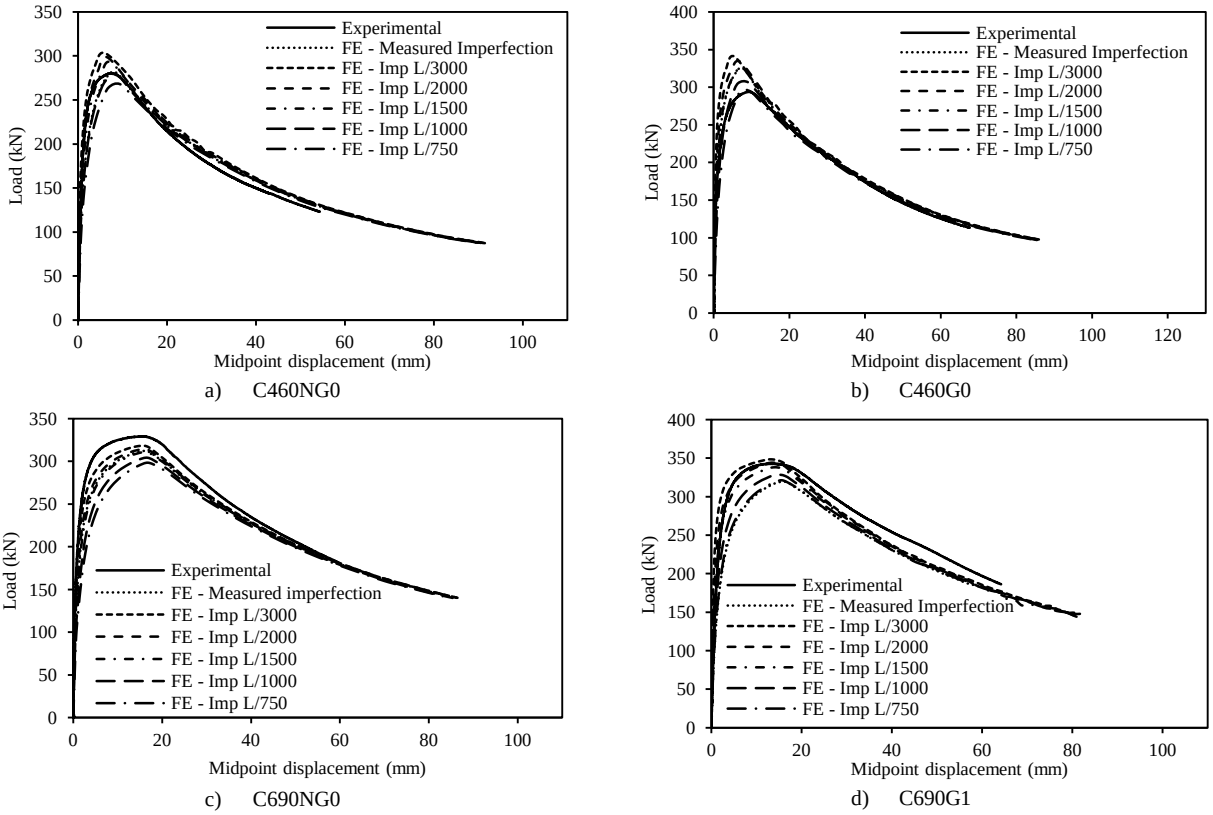


Figure 4. Compressive specimens - Comparison of numerical and experimental load-deformation response for six geometric imperfection magnitudes.

### 3.3 Failure modes

In addition to the comparison of the experimental to FE ultimate loads and load-deformation curves, the failure modes were also successfully replicated. Figure 5 depicts representative numerically obtained failure modes for the tensile (i.e. necking) and compressive (i.e. global buckling) members. Note that even though no material damage has been introduced in the models, necking has been successfully captured, demonstrating the previously drawn conclusion that necking formation is also related to geometric instabilities [12].

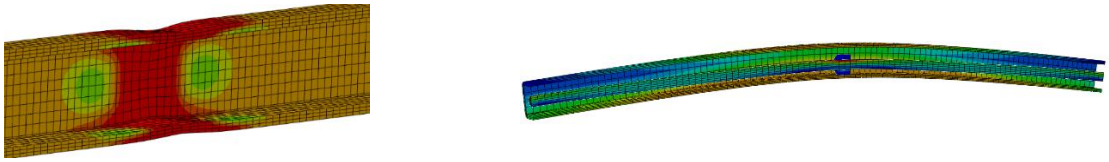

a) Necking - Tensile specimens b) Buckling - Compressive specimens

Figure 5. Failure modes.

### 3.4 Discussion

Having successfully validated the FE models, the obtained numerical results are summarized in Figure 6, where the ultimate loads are plotted against the prestress level, given as a percentage of the cable's squash load. Note that 0% prestress in the horizontal axis of Figure 6(a) corresponds to a tensile member without any cable. As can be seen in Figure 6(a), the introduction of prestress increases considerably the ultimate performance of tensile members. A slightly increased ultimate load can be offered with the addition of grouting. Additionally, Figure 6(b) shows that the introduction of initial compressive stresses to the tube decreases its ultimate load under compression. A noticeable improvement in the performance can be achieved with the addition of concrete, owing to its enhanced compressive resistance.

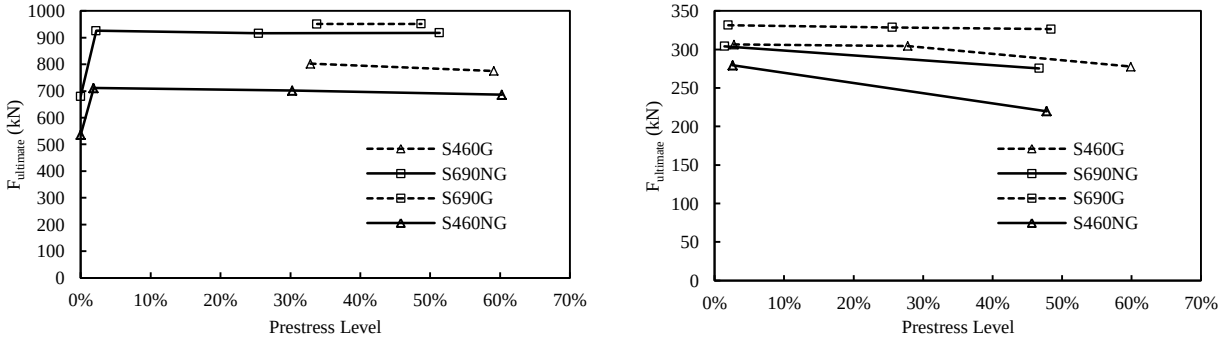


a) Tensile b) Compressive (imperfection magnitude: $L$/1000)

Figure 6. Summary - Obtained numerical results.

## 4 SUMMARY - CONCLUSIONS

The present paper investigated the compressive and tensile response of prestressed members employing S460 and S690 square hollow sections by means of numerical modelling. The generated finite element models were comprehensively discussed. The FE results were compared to the test data provided in [1]. Four prestress levels including a member without any cable, a member with a cable in $P_{nom}$ prestress, in $0.5P_{opt}$ and $P_{opt}$ prestress were examined. The numerically obtained ultimate load and load-deformation response were compared with the experimental ones, revealing a successful validation. The failure modes were also successfully replicated. Overall it was shown that prestressing can improve the structural performance of tensile members, while the addition of

grouting could contribute to an improved performance. For members subjected to compressive axial loading, the introduction of initial compressive stresses to the tube causes the onset of global buckling at a lower load.

**REFERENCES**

[1] Wang, J., Afshan, S. and Gardner, L. (2016), "Axial behaviour of prestressed high strength steel tubular members" *Proceedings of the international colloquium on stability and ductility of steel structures – SDSS 2016*, 30 May-01 June 2016, Timisoara, Romania.
[2] S-Squared (2017), "Creators of super powerful structures [online]", Available from: http://www.s-squared.com.au/home.aspx [Accessed 7 January 2017].
[3] Gosaye, J., Gardner, L., Wadee, M.A. and Ellen, M.E. (2014), "Tensile performance of prestressed steel elements", *Engineering Structures*, Vol. 79, pp. 234-243.
[4] Gosaye, J., Gardner, L., Wadee, M.A. and Ellen, M.E. (2016), "Compressive behaviour and design of prestressed steel elements", In *Structures*, Vol. 5, pp. 76-87.
[5] Gkantou, M., Theofanous, M. and Baniotopoulos, C. (2016), "On the structural response of high strength steel prestressed trusses. A numerical approach." *Proceedings of 11th HSTAM International Congress on Mechanics*, 28-30 May 2016, Athens, Greece.
[6] Wang, J., Afshan, S., Gkantou, M., Theofanous, M., Baniotopoulos, C. and Gardner, L. (2016), "Flexural behaviour of hot-finished high strength steel square and rectangular hollow sections", *Journal of Constructional Steel Research*, Vol. 121, pp. 97-109.
[7] Hibbitt, Karlsson and Sorensen Inc (2010), "ABAQUS, ABAQUS/Standard user's manual", Pawtucket, USA.
[8] Gardner, L. and Nethercot, D.A. (2004), "Experiments on stainless steel hollow sections - Part 1: Material and cross-sectional behaviour," *Journal of Constructional Steel Research*, Vol. 60 (9), pp.1291-1318.
[9] Manos, G.C., Theofanous, M. and Katakalos, K. (2014), "Numerical simulation of the shear behaviour of reinforced concrete rectangular beam specimens with or without FRP-strip shear reinforcement", *Advances in Engineering Software*, Vol. 67, pp. 47-56.
[10] ACI. Committee 318. (1999), "Building code requirements for structural concrete and commentary (ACI 318-99)", Detroit (MI): American Concrete Institute.
[11] Abdullah, A.B.M., Rice, J.A., Hamilton, H.R. and Consolazio, G.R. (2016), "An investigation on stressing and breakage response of a prestressing strand using an efficient finite element model", *Engineering Structures*, Vol. 123, pp. 213-224.
[12] Okazawa, S., Usami, T., Noguchi, H. and Fujii, F. (2002), "Three-dimensional necking bifurcation in tensile steel specimens", *Journal of engineering mechanics*, Vol. 128(4), pp. 479-486.